ADVANCED PILOT MODELING FOR ROTORCRAFT HANDLING QUALITIES INVESTIGATION IN TURBULENT WIND

Honglei Ji, jhl@cqu.edu.cn, Chongqing University (China)
Linghai Lu, L.Lu@cranfield.ac.uk, Cranfield University (United Kingdom)

Abstract
Turbulent wind is known notoriously that can significantly deteriorate rotorcraft performance and handling qualities for manoeuvring flight. However, research on this topic is rarely reported largely due to the lack of an effective analytical tool. This paper develops a pilot model to explore the effect of turbulent wind on rotorcraft handling qualities. The proposed pilot model consists of three components: a compensatory control model for attitude stabilization, a preview control model for trajectory tracking, and a tau guidance model for trajectory planning. Model accuracy assessment indicates that the new pilot model can plan and track a desired trajectory conforming to pilot's tau guidance strategy and predict credible handling qualities capturing the effect of the vestibular system and a flight control system. Handling qualities analysis for a slalom task in turbulent wind shows that the new pilot model predicts the effect of mean wind on rotorcraft manoeuvring aggressiveness and yaw control performance by changing required ground speed and the airflow through the tail rotor. Atmospheric turbulence significantly deteriorates the task with increased turbulence intensities. Flight control system can significantly improve the tracking performance and HQs in turbulent wind but saturation due to limited authority in aggressive operation reduces the effect of the flight control system.

1. INTRODUCTION

Rotorcraft nap-of-the-earth manoeuvres encountering turbulent wind are considered demanding tasks. Under these kinds of circumstances, a pilot could be distracted from manoeuvring operations to disturbance rejection, resulting in deteriorated performance and Handing Qualities (HQs)[1]. The effect of turbulent wind on HQs still presents a severe problem for rotorcraft applications although a variety of turbulence models have been developed from physics- or data-based modelling methods[2-5]. Developing a pilot model is urgently necessary not only for the prediction and explanation of adverse rotorcraft responses in turbulent wind[1] but also to reduce time and cost through design and development to certification, training and operations of a prototype rotorcraft[6].

Pilot modelling techniques[7-14] have been widely developed for flight simulation and HQs investigation. Hess[12,15-17] proposed the structural pilot model for rotorcraft manoeuvring simulations, handling qualities and adverse man-machine coupling prediction, as well as flight simulator fidelity assessment as early as the 1980s. The model has a compensatory structure with elements to simulate proprioceptive, vestibular, and visual systems of a human pilot, and the parameters are tuned by matching the crossover frequency. The pilot model functioned as a controller to track a predefined trajectory to complete the simulation of selected Mission Task Elements (MTE), such as slalom, lateral reposition, acceleration/deceleration et al.[15, 18]. A metric for HQs evaluation, referred as the Handling Qualities Sensitivity Function (HQSF)[16], was calculated from the simulated proprioceptive feedback signals, and thus the task-dependent HQs could be evaluated for the specific MTEs[12]. Other pilot models were also developed for rotorcraft manoeuvring simulations, such as using the precision model[19] and optimal control model[20] for a recovery task in ship airwake. The preceding models share a common feature – both need a predefined flight path, which usually takes the form of a high-order polynomial[21]. A question naturally arises that whether the flight path conforms to a pilot's control strategy. This is a difficult but very important question in that the predefined flight path may affect the handling qualities. For example, in a side-step manoeuvre the shape of the acceleration profile indicated the attitude quickness[22]. Recent research [23-27] in the biologically inspired optic flow theory may give a satisfactory answer.

Inspired by humans and animals perceiving the instantaneous time from the available optic flow to approach a target, tau theory defined a time-to-contact variable, called the tau (τ), to describe the relationship between the close gap and close rate[23-

24]. The variation of the tau could be used to guide a motion through a so-called tau-coupling[23]. The τ-guide control strategies have been demonstrated from a series of rotorcraft manoeuvres in piloted simulations, such as quick stop, level turn, and hill climb to avoid a hazard[25-26]. Lu et al.[13,27] successfully used τ as a mechanism and control variable to model a pilot's guidance and avoidance strategy to deal with the impeding hazards. All above results demonstrate the tau theory as a potential strategy for trajectory planning, and therefore, the last problem is how to accurately track a predefined trajectory. It has been long known that pilot previewed the desired future path to generate present control inputs for rotorcraft operations involving low-altitude manoeuvring flight, which is the so-called preview control strategy[12]. Recent research[14] further confirmed that humans used a previewed target trajectory to improve tracking performance primarily due to the far-viewpoint response. It allows humans to cancel their own and the controlled element's lags without additional activity.

A pilot normally performs both stabilization and guidance functions simultaneously when low-altitude manoeuvring flight[27]. The current pilot models focused on either the stabilization function or the guidance function, but none organically combined both of the two functions. The proposed research in this paper extends to develop a pilot model to investigate the effect of turbulent wind on rotorcraft manoeuvring HQs. Section 2 will give a brief introduction to the simulation model including a turbulent wind model and a flight dynamics model. Section 3 describes the pilot model sequentially with the control strategy, preview control model and tau guidance model. Section 4 illustrates the experimental setup for the MTE, turbulent wind conditions, and the development of a flight control system. Section 5 gives the methodology for HQs analysis and assesses the accuracy of the proposed pilot model for manoeuvring flight simulation. In section 6 the effect of turbulent wind on rotorcraft HQs is systematically investigated from the effect of mean wind and atmospheric turbulence to the effect of a flight control system. The results of the simulations are discussed and concluded in Sections 7 and 8, respectively.

2. SIMULATION MODEL

Figure 1 shows the simulation frame for rotorcraft manoeuvring flight in turbulent wind. The simulation model used in this paper consists of two components: a low-altitude turbulent wind model and a rotorcraft flight dynamics model and the details have been given in Refs. [1, 3-5]. The incorporated turbulent wind and flight dynamics model has been validated against the flight test data in bluff-body turbulence and freestream turbulence. More details about the validation and applications of the simulation model could be found in Refs. [3-5]. Here a brief introduction will be given.

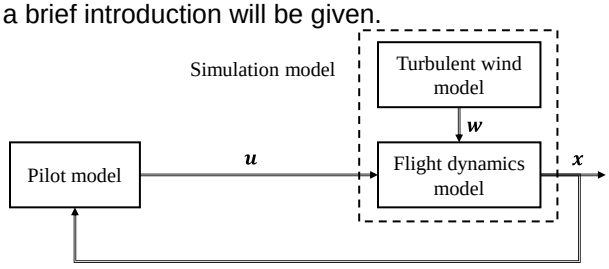

Fig. 1 Simulation frame for manoeuvring flight in turbulent wind

The instantaneous velocity of turbulent wind was formulated with a mean wind velocity and a turbulence velocity. The mean wind velocity was assumed invariable with time and space. The magnitude of the mean wind velocity was formulated by the wind profile power law[28] and the exponent is an empirically derived coefficient varying dependent upon the underlying terrain roughness[29]. The mean wind velocity components were calculated by transforming the mean wind magnitude into the North-East-Down (NED) axes with the wind direction angle. The turbulence velocity was assumed randomly varying spatially on the basis of the 'frozen field hypothesis'[30]. The distributed turbulence model [3-5] was employed to provide a three-dimensional turbulence field covering each aerodynamic surface of the object rotorcraft. The turbulence components for each aerodynamic surface were calculated with the nearest interpolation to the turbulence field and were summed with the mean wind velocity components for incorporation with the flight dynamics model.

The mathematical model from Ji et al.[19] describes a generic UH-60A helicopter. The effect of atmospheric turbulence on aircraft aerodynamics is considered by superimposing the turbulence disturbances directly to the local inflow velocities of the main rotor blade segments, fuselage, horizontal stabilator, vertical fin, and tail rotor. The incorporated distributed turbulence model and rotorcraft flight dynamics model can be expressed as,

$$(1)\ \dot{\boldsymbol{x}} = f(\boldsymbol{x}, \boldsymbol{u}, \boldsymbol{w}, t)$$

where $\boldsymbol{x}$ is the state vector of motion,

$$\boldsymbol{x} = \begin{pmatrix} u, v, w, p, q, r, \Phi, \Theta, \Psi, \dot{\beta}_1, \dot{\beta}_2, \dot{\beta}_3, \dot{\beta}_4, \beta_1, \beta_2, \beta_3, \\ \beta_4, \dot{\zeta}_1, \dot{\zeta}_2, \dot{\zeta}_3, \dot{\zeta}_4, \zeta_1, \zeta_2, \zeta_3, \zeta_4, \dot{\theta}_{\mathrm{dyn}}, \theta_{\mathrm{dyn}}, v_{\mathrm{i}}, v_{1\mathrm{c}}, \\ v_{1\mathrm{s}}, v_{\mathrm{itr}}, v_x, v_y \end{pmatrix}^T$$

where u, v, w, p, q, r are the linear velocity components and angular rates of the fuselage. Φ, Θ, Ψ are the Euler angles. $\dot{\beta}_1, \dot{\beta}_2, \dot{\beta}_3, \dot{\beta}_4, \beta_1, \beta_2, \beta_3, \beta_4$ are the flapping angular rates and angles of the four rigid blades. $\dot{\varsigma}_1, \dot{\varsigma}_2, \dot{\varsigma}_3, \dot{\varsigma}_4, \varsigma_1, \varsigma_2, \varsigma_3, \varsigma_4$ are the lagging angular rates and angles. $\theta_{\mathrm{dyn}}, \dot{\theta}_{\mathrm{dyn}}$ are the blade tip dynamic torsion angle and angular rate. $v_{\mathrm{i}}, v_{1\mathrm{c}}, v_{1\mathrm{s}}$ are the main rotor induced velocities. v_{itr} is

the tail rotor induced velocity. v_x and v_y are the delayed fuselage downwash and sidewash components, respectively. $\boldsymbol{u}$ is four rotorcraft controls,

$$\boldsymbol{u} = \left(\delta_{\mathrm{col}}, \delta_{\mathrm{lat}}, \delta_{\mathrm{lon}}, \delta_{\mathrm{ped}}\right)^T$$

where δ_{col} is collective input, δ_{lat} is lateral cyclic stick input, δ_{lon} is longitudinal cyclic stick input, and δ_{ped} is pedal input. $\boldsymbol{w}$ is the turbulence disturbances,

$$\mathbf{w} = \begin{pmatrix} U_{\mathrm{i,j}}, V_{\mathrm{i,j}}, W_{\mathrm{i,j}}, U_{\mathrm{fs}}, V_{\mathrm{fs}}, W_{\mathrm{fs}}, U_{\mathrm{hs}}, V_{\mathrm{hs}}, W_{\mathrm{hs}}, U_{\mathrm{vt}}, V_{\mathrm{vt}}, \\ W_{\mathrm{vt}}, U_{\mathrm{tr}}, V_{\mathrm{tr}}, W_{\mathrm{tr}} \end{pmatrix}^{\mathrm{T}}$$

where $U_{\mathrm{i,j}}, V_{\mathrm{i,j}}, W_{\mathrm{i,j}}$ are the instantaneous wind components at the jth segment, ith blade of the main rotor, $U_{\mathrm{fs}}, V_{\mathrm{fs}}, W_{\mathrm{fs}}$ are the instantaneous wind components at the fuselage, $U_{\mathrm{hs}}, V_{\mathrm{hs}}, W_{\mathrm{hs}}$ are the instantaneous wind components at the horizontal stabilator, $U_{\mathrm{vt}}, V_{\mathrm{vt}}, W_{\mathrm{vt}}$ are the instantaneous wind components at the vertical fin, and $U_{\mathrm{tr}}, V_{\mathrm{tr}}, W_{\mathrm{tr}}$ are the instantaneous wind components at the tail rotor. t represents the time in seconds.

3. PILOT MODEL

3.1. Scheme of Proposed Pilot Model

The pilot control activities could be divided into three functions: stabilization, guidance, and navigation[27]. Only the latter two functions were activated by a pilot for rotorcraft manoeuvring tasks such as the MTEs defined in the rotorcraft HQs performance specification ADS-33[31]. Figure 3 shows the proposed pilot control strategy. Hess's compensatory pilot model[8,16] is employed for attitude stabilization. On this basis, a preview control model is developed for trajectory stabilization and tracking. Here, preview control[15] indicates that the pilot can preview the desired future flight trajectory and both the current and future values of the desired trajectory are used to improve tracking performance. The desired trajectory is provided by a tau guidance model to conform to the guidance strategy that a normal pilot would try to achieve.

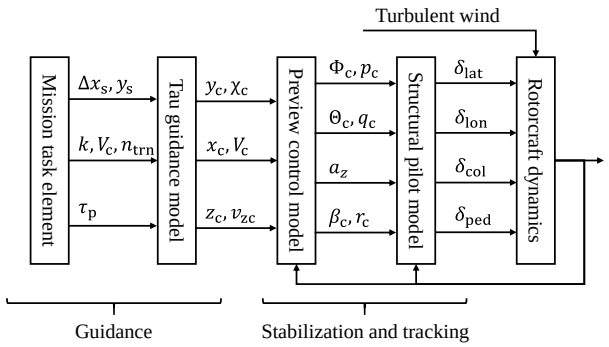

Fig. 2 Control strategy for rotorcraft manoeuvre in turbulent wind

3.2. Structural Pilot Model

The structural pilot model by Hess is chosen for attitude control in that the model created is not only able to describe compensatory pilot behaviour, but can account for visual, proprioceptive, and vestibular cues in an approximate fashion[12,15-18]. As a starting point, the structure of the pilot model for roll attitude control is illustrated in Fig. 3. The visual loop is closed because the pilot rely mostly on the visual cues to track the desired attitude C, which refers to the desired roll angle Φ_{c} for this case. This loop deals with the tracking attitude error e_Φ between the desired roll angle Φ_{c} and the feedback roll angle Φ through the gain variable K_Φ. The control signal is transferred to the desired derivative $\dot{C}$ after the time-delay element $e^{-\tau s}$ accounting for the pilot's cognitive responsiveness. The following visual model[18] is injected between the attitude error e_Φ and the gain variable K_Φ to reflect the quality of visual information sensed by the pilot,

$$(2) e'_\Phi = e_\Phi \left(1 + \eta \frac{1}{0.5s + 1}\right)$$

where e and e' are the true and observed values of the visual error signal, as well as η is the band-limited white noise with a unit intensity, which is saturated with limits of $2\sigma_\eta^2$.

In addition to the visual loop, the pilot usually combines the proprioceptive and vestibular loops to enhance stability and tracking performance. The weighted combination of the proprioceptive and vestibular signals are adopted as the feedback roll rate $\hat{p}$ with the weighting coefficients λ_1 and λ_2. The roll rate error e_p between the desired roll rate $\dot{C}$ and the feedback roll rate $\hat{p}$ is multiplied by the gain variable K_p to produce the control signal δ. The proprioceptive signal U_M is produced from the pilot's internal model $\hat{p}/\delta_{\mathrm{lat}}$ while the vestibular signal is sensed directly from the vehicle motion cues. Additional vestibular signal p_{c} for coordination with the other channels may also be included to estimate the feedback roll rate with the weighted coefficient λ_3.

The control signal δ is applied by the neuromuscular system G_{nm} of the pilot to the cockpit force/feel system G_{fs} to produce the lateral stick input δ_{lat}. The neuromuscular system G_{nm} is modelled as a second-order transfer function by neglecting very high-frequency input information[16],

$$(3)\ G_{\mathrm{nm}} = \frac{\omega_{nm}^2}{s^2 + 2\omega_{nm}\zeta_{nm}s + \omega_{nm}^2}$$

where ω_{nm} and ζ_{nm} are the natural frequency and damping ratio.

The successful implementation of the structural pilot model depends upon a sensible selection of the pilot parameters in Fig. 3. Moreover, the pilot model, constructed with those parameters, needs to satisfy at least two requirements. First, the final pilot model should be able to perform the required tracking task. Second, the pilot model should match the real behaviour of a pilot as closely as possible. To meet these requirements, the gain K_p is chosen such that

all of the dampling ratios of the closed-loop proprioceptive system are larger than 0.15, and the gain K_Φ is selected so that the open-loop crossover frequency of the visual system is equal to 2 rad/s, which is a representative value of high-gain pilot control activity derived from flight-test data[12]. The variance of the visual noise σ_η^2 is chosen as 0.1 to achieve a level-1 useable cue environment, and the cognitive delay τ takes a typical value of 0.2 s. The proprioceptive system transfer function is designed by a lowest-order approximation to the vehicle rate dynamics near the region of crossover frequency. The weighted coefficients λ_1 and λ_2 take a 0.75/0.25 split[17-18] to reflect the degree of the importance between the proprioceptive and vestibular channels when the motion cues are available, and take a 1/0 split when the motion cues are off. The additional vestibular signal takes the same weight as the on-axis vestibular signal. The neuromuscular damping ratio ζ_{nm} and natural frequency ω_{nm} are selected as typical values of 0.707 and 10 rad/s[12] and the cockpit force/feel system dynamics is selected as,

$$(4)\ Y_{\mathrm{NM}} = \frac{625}{s^2 + 35.35s + 625}$$

The longitudinal, heave, and yaw channels can be designed by following the same procedure. The pitch angle Θ and pitch rate q are taken as the visual and vestibular feedback signals for pitch attitude control. The sideslip angle β and heading rate r are used in the yaw axis and the vertical speed v_z and acceleration a_z in the vertical axis. The desired visual signals and the additive vestibular signals will be given by the preview control model.

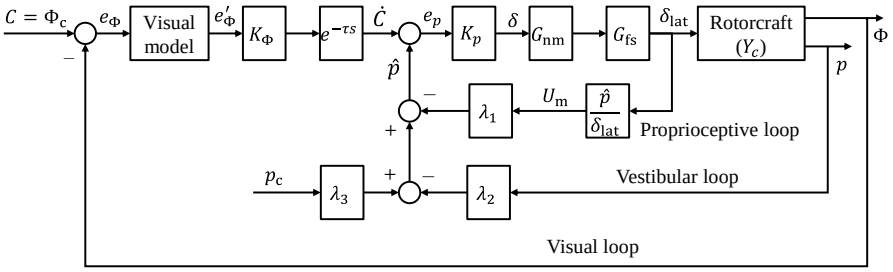

Fig. 3 Structural pilot model for roll attitude control

3.3. Preview Control Model

The preview control model combines trajectory tracking and turn coordination techniques. The trajectory tracking law uses both current and future values of the desired trajectory as well as the current vehicle position and velocity to produce desired visual signals (attitudes) for the inner-loop compensatory pilot model. The turn coordination law produces desired vestibular signals (angular rates and vertical acceleration) according to equilibrium in the forces.

3.3.1. Trajectory tracking law

The ground speed V, course angle χ, and vertical position z are taken as the reference signals for trajectory tracking in longitudinal, lateral, and vertical axes. The lateral axis is used to illustrate the development.

Figure 4 shows the preview control model for lateral trajectory tracking, where χ_c and χ are the desired and current course angles, e_y is the lateral position error, τ_p is the pilot preview time, as well as K_χ, K_{χ_p}, and K_y are the feedback gains. A feedforward preview of the desired course angle is introduced to compensate for the inherent delays in the man/machine system[15]. Furthermore, the lateral position error is also fed back to improve the position tracking precision. The longitudinal and lateral position errors are calculated by,

$$(5)\ \begin{pmatrix} e_x \\ e_y \end{pmatrix} = \begin{bmatrix} \cos\chi & \sin\chi \\ -\sin\chi & \cos\chi \end{bmatrix} \begin{pmatrix} x_c - x \\ y_c - y \end{pmatrix}$$

where e_x and e_y are the longitudinal and lateral position errors, x and y are the position coordinates of the controlled vehicle in the NED axes, as well as x_c and y_c are the desired position coordinates in the NED axes.

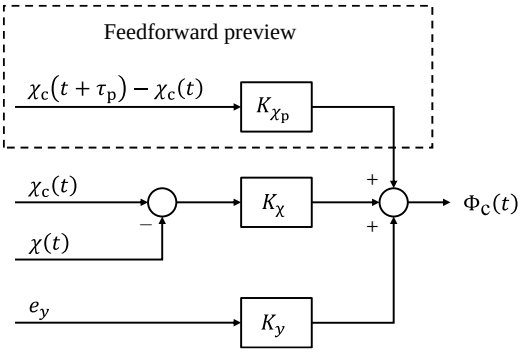

Fig. 4 Preview control model for lateral trajectory tracking

The control law in Fig. 4 is defined for the lateral trajectory tracking,

$$(6)\ \Phi_c(t) = K_\chi[\chi_c(t) - \chi(t)] + K_{\chi_p}[\chi_c(t+\tau_p) - \chi_c(t)] + K_y e_y$$

where the preview gain K_{χ_p} is chosen as the same as the compensatory gain K_χ to achieve a good level

of tracking performance. As consequence, the preview control law in Eq. (6) is simplified as,

$$(7)\ \Phi_{\mathrm{c}} = K_{\chi}\left[\chi_{c}\left(t+\tau_{\mathrm{p}}\right)-\chi(t)\right]+K_{y}e_{y}$$

The pilot gain K_{χ} is designed to obtain the desired crossover frequency $\omega_{\mathrm{c}\chi}$ for the course angle tracking. According to the rules for multi-loop pilot models[18], $\omega_{\mathrm{c}\chi} = 1/3\,\omega_{\mathrm{c}\Phi}$ is a good rule of thumb. The pilot gain K_{y} is designed to obtain the desired crossover frequency $\omega_{\mathrm{c}y}$ for lateral position tracking. The value of $\omega_{\mathrm{c}y}$ is chosen as 1/5 the value of $\omega_{\mathrm{c}\chi}$. Thus, the preview control model for the lateral trajectory tracking has been formed.

Following the rule of the lateral case, the control law employing the ground speed as the control signal for longitudinal trajectory tracking is,

$$(8)\ \Theta_{\mathrm{c}} = K_{V}\left[V_{\mathrm{c}}\left(t+\tau_{p}\right)-V(t)\right]+K_{x}e_{x}$$

where K_{V} and K_{x} are the pilot gains for ground speed and position tracking, $V_{\mathrm{c}}\left(t+\tau_{\mathrm{p}}\right)$ is the previewed ground speed at the time $t+\tau_{\mathrm{p}}$, as well as $V(t)$ is the current vehicle ground speed at the time t.

The pilot control law for vertical trajectory tracking is,

$$(9)v_{\mathrm{zc}} = K_{z}\left[z_{\mathrm{c}}\left(t+\tau_{\mathrm{p}}\right)-z(t)\right]$$

where K_{z} is the pilot gain, $z_{\mathrm{c}}\left(t+\tau_{\mathrm{p}}\right)$ is the previewed vertical position at the time $t+\tau_{\mathrm{p}}$, as well as $z(t)$ is the current vertical position at the time t.

3.3.2. Turn coordination law

To enter a turn from straight-and-level flight, a human pilot will apply lateral control input in the same direction the turn is to be made[32]. The pedals are only used to compensate for torque to keep the rotorcraft in trim around the vertical axis rather than to assist the turn directly[33]. Keeping the fuselage in the correct streamlined position without sideslip around the vertical axis facilitates the rotorcraft flying forward with the least drag, that is

$$(10)\beta_{\mathrm{c}} = 0$$

Lateral trim is indicated by a centred ball on a turn and slip indicator to remove sideslip[32]. Recalling the lateral force equation[34],

$$(11)\dot{v} = -ur + wp + g\cos\Theta\sin\Phi + \frac{F_{y}}{m}$$

where g is the gravitational acceleration; F_{y} is the external lateral force excluding the gravitational force in the body axes; m is the aircraft mass.

Lateral acceleration that will feed to the pilot as a vestibular cue will become larger as the roll and sideslip angles increase, as indicated in Eq. (11). The pilot corresponds to adopting a compensatory control for the coupled yaw to remove the lateral acceleration, that is

$$(12)\ \dot{v} \approx 0$$

The vertical velocity w and roll rate p are much smaller compared to the longitudinal velocity u. Therefore, the wp term is negligible when solving the desired yaw rate from Eq. (11), which is,

$$(13)r_{\mathrm{c}} = \frac{1}{u}\left(g\cos\Theta\sin\Phi + \frac{F_{y}}{m}\right)$$

Furthermore, considering a steady level turn with the turn rate Ψ, the time rate of change of the roll and pitch angles should be zero,

$$(14)\dot{\Phi} = \dot{\Theta} = 0$$

Thus, the relationship between the fuselage angular rates in the body axes and the time rate of change of the attitude angles is simplified as,

$$(15)\begin{cases} q = \Psi\cos\Theta\sin\Phi \\ r = \Psi\cos\Theta\cos\Phi \end{cases}$$

From Eq. (15), the desired pitch rate has the following relationship with the desired yaw rate,

$$(16)q_{\mathrm{c}} = r_{\mathrm{c}}\tan\Phi$$

Since the pilot will always remove sideslip in forward flight, the external force F_{y} is negligible when solving the desired pitch rate. Therefore, the desired pitch rate for the longitudinal vestibular system is,

$$(17)q_{\mathrm{c}} = \frac{g\cos\Theta\sin\Phi\tan\Phi}{u}$$

Finally, the main rotor force vector will tilt along with the bank of the rotorcraft during a level turn, and as a consequence, compensation is required for height hold. Recalling the vertical force equation[34],

$$(18)\ \dot{w} = uq - vp + g\cos\Theta\cos\Phi + \frac{F_{z}}{m}$$

where F_{y} is the vertical force excluding the gravitational component in the body axes.

Neglecting the small term vp and substituting the desired pitch rate q_{c}, the vertical acceleration is obtained for the vertical vestibular system,

$$(19)\ a_{z} = uq_{\mathrm{c}} + g\cos\Theta\cos\Phi + \frac{F_{z}}{m} = \frac{g\cos\Theta}{\cos\Phi} + \frac{F_{z}}{m}$$

It can be found that pilots use a combined tracking/compensatory control strategy to achieve a steady coordinated turn in forward flight. The primary control is centred on the lateral axis and the compensation control activities in the other three axes are required to reduce unwished rotorcraft responses suffering from inter-axis coupling and atmospheric disturbances.

3.4. Tau Guidance Model

Tau theory is based upon the fundamental parameter τ_{x}, which is the time-to-contact variable in the optical field[23],

$$(20)\ \tau_{x} = \frac{x}{\dot{x}}$$

where x is the perceived (negative) motion gap to be closed, and $\dot{x}$ is the instantaneous gap closure rate.

The tau of a gap is essentially the time it will take until the gap is reduced to zero at the current rate. The gap can be either a spatial gap (such as distance, angle) or a forced gap. In this paper, spatial gaps are under investigation. Lee[24] hypothesized that the tau of a motion gap is coupled to an intrinsic tau guide τ_{g},

$$(21)\ \tau_{\chi} = k\tau_{g}$$

where x is the externally perceived spatial variable, k is the coupling constant, τ_g is the intrinsic tau guide, and both τ_x and τ_g vary with time.

The intrinsic tau guide τ_g defines a motion that is guiding a moving target with its tau. It can take a number of different forms, but the most interesting and relevant is the constant acceleration guide. This can be used to guide the motion of an object that is approaching or receding from a target and that starts at rest or starts with some initial velocity[24]. The constant acceleration tau guide is given as,

$$(22)\ \tau_g = \frac{t(T+t)}{T+2t}$$

where T is the total motion duration and t is the current time during the motion.

When coupled onto such a guide, the motion starting at rest to approach a target can be derived from the relationship in Eq. (21) [27],

$$(23)\ \begin{cases} \tilde{x} = -(1-\tilde{t}^2)^{\frac{1}{k}} \\ \tilde{x}' = \frac{2}{k}\tilde{t}(1-\tilde{t}^2)^{\frac{1}{k}-1} \\ \tilde{x}'' = \frac{2}{k}\left[1-\left(\frac{2}{k}-1\right)\tilde{t}^2\right](1-\tilde{t}^2)^{\frac{1}{k}-2} \end{cases}$$

where $\tilde{x}$ and $\tilde{t}$ are the normalized spatial gap and time by the initial gap x_0 and the total motion duration T, respectively; $\tilde{x}'$ and $\tilde{x}''$ are the first- and second-derivatives of the normalized gap $\tilde{x}$ to the normalized time $\tilde{t}$.

Inspection of the constant acceleration τ_g guide equations in (23) reveals that the coupling constant k will provide differing responses when approaching a target[35], as showing in Fig. 5. A value of $k < 0.5$ results in an acceleration-deceleration motion with zero residual speed. Furthermore, there are two maximum accelerations during the approaching motion: one is at the beginning to initiate the manoeuvre and the other is at a later time to stop it. The first maximum acceleration decreases with the increased coupling constant k. However, the second maximum acceleration decreases with the increment of k when $k < 0.4$, while increases when $k > 0.4$, and achieves a minimum peak value when $k = 0.4$. Since the maximum acceleration decides the aggressiveness of a motion[22], a value of 0.4 is selected as the best for HQs, which was demonstrated by a series of pilot-in-the-loop simulation experiments[26].

The ADS-33 slalom MTE[31] is taken as an example to present the trajectory planning procedure using the tau guide. The manoeuvre is started with a constant velocity along a centreline, followed by a series of smooth turns to the left and right in sequence, and completed by regaining the centreline, as shown in Fig. 6. Experiments demonstrated that pilots picked up visual information from look-ahead points and used the tau guidance strategy adapting to changing cues and task demands for manoeuvring flight[25,36]. For the slalom task, when a turn is performed the pilot will move the reference point to the next turn to get a new motion gap. Therefore, taking the turns as the reference points, every piece of the flight path between adjacent turns can be planned following the tau guidance strategy. Supposing the number of the turns to each side of the centreline is n_{trn}, the flight path can be cut into $2n_{trn}+1$ segments. The coordinates of the ith reference point are expressed as (x_i, y_i) and those at the starting and ending locations are expressed as (x_0, y_0) and $\left(x_{2n_{trn}+1}, y_{2n_{trn}+1}\right)$, subjective to the following relationship,

$$(24)\ x_{i+1} = x_i + \Delta x_{\mathrm{s}}$$

$$(25)\ |y_i| = y_{\mathrm{s}}$$

where Δx_{s} is the spatial interval between the adjacent turns, and y_{s} represents the lateral distance from the centreline.

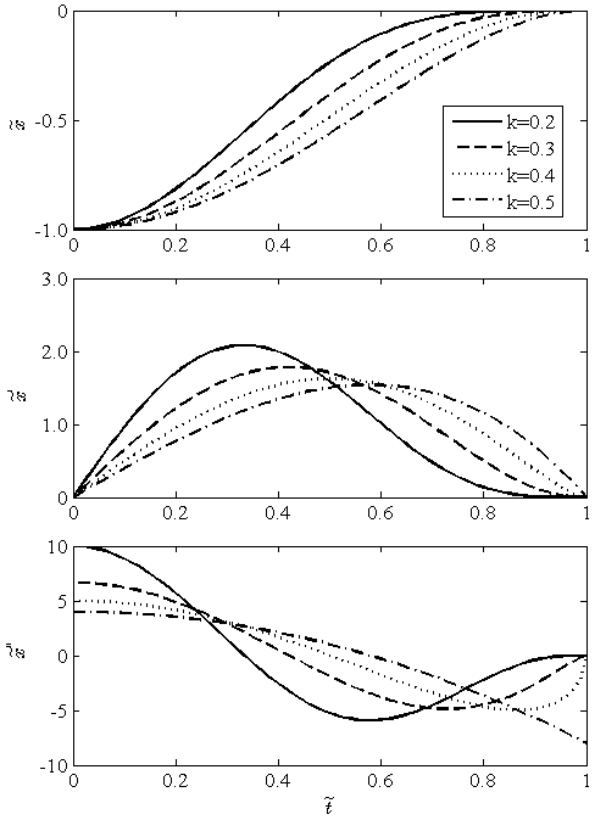

Fig. 5 Gap distance, closure rate and acceleration of constant acceleration guide

Supposing the desired ground speed is V_{c}, the duration to pass through the first and last segments is,

$$(26)\ \Delta t_1 = \frac{\sqrt{y_s^2 + \Delta x_s^2}}{V_{\mathrm{c}}}$$

The duration across the other segments is,

$$(27)\ \Delta t_2 = \frac{\sqrt{(2y_s)^2 + \Delta x_s^2}}{V_{\mathrm{c}}}$$

Supposing the initial time is t_0, the time when the vehicle just passing through the ith reference point is

$$(28)\ t_i = \begin{cases} t_0 + \Delta t_1, & i = 1 \\ t_1 + (i-1)\Delta t_2, & i = 2, \cdots, 2n_{trn} \\ t_{2n_{trn}} + \Delta t_1, & i = 2n_{trn} + 1 \end{cases}$$

As consequence, the dimensionless time $\tilde{t}$ during the ith segment is,

$$(29)\ \tilde{t} = \begin{cases} (t - t_i)/\Delta t_1\,, & t < t_1 \ or \ t > t_{2n_{trn}} \\ (t - t_i)/\Delta t_2\,, & t_1 \le t \le t_{2n_{trn}} \end{cases}$$

According to Eq. (23), the dimensionless lateral velocity $\tilde{v}_{yc}$ is,

$$(30)\ \tilde{v}_{yc} = \frac{2}{k}\tilde{t}(1 - \tilde{t}^2)^{\frac{1}{k}-1}$$

Correspondingly, the desired lateral velocity v_{yc} for the slalom MTE is,

$$(31)\ v_{yc} = \tilde{v}_{yc} \cdot \begin{cases} y_s/\Delta t_1\,, & t < t_1 or t > t_{2n_{trn}} \\ -y_s/\Delta t_2\,, & t_{2j} < t < t_{2j+1} \\ y_s/\Delta t_2\,, & t_{2j+1} < t < t_{2(j+1)} \end{cases}$$

where $j = 1,2,\cdots,n_{trn}$.

Provided with the constant ground speed V_c, the desired longitudinal velocity v_{xc} is,

$$(32)\ v_{xc} = \sqrt{V_c^2 - v_{yc}^2}$$

Therefore, the desired course angle χ_c is,

$$(33)\ \chi_c = \arctan\frac{v_{yc}}{v_{xc}}$$

The slalom MTE requires a constant height, and so the vertical velocity is always zero. Thus, the desired trajectory can be produced by integrating the desired velocities over time.

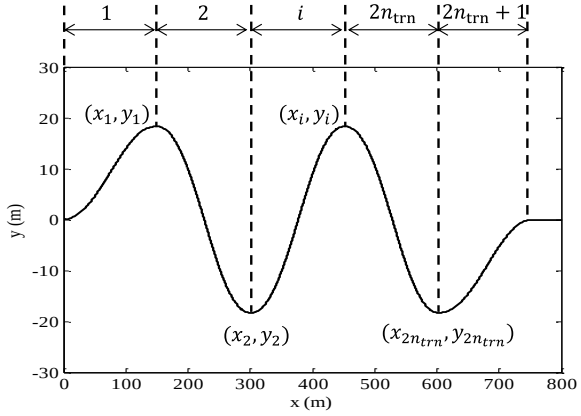

Fig. 6 Selected reference points for slalom trajectory tracking

4. EXPERIMENT SETUP

4.1. Mission Task Element

The slalom MTE [31] is selected for handling qualities analysis. It is intended to check the lateral-directional coordination during an aggressive manoeuvre in forward flight with respect to cones on the ground. The task consists of a series of smooth turns at 500-ft (about 150 m) intervals below the reference altitude of 100 ft (about 30 m) as shown in Fig. 7. The turns shall be at least twice to each side of the course and at least 50 ft (about 15 m) from the centreline, with the maximum lateral error of 50 ft (about 15 m). The desired performance requires an airspeed of at least 60 knots (about 30 m/s) throughout the course and the adequate performance is at least 40 knots (about 20 m/s).

The UH-60A helicopter is employed for all simulated cases as shown in Table 1. Following the ADS-33E's requirements, the desired lateral distance from the centreline is set as 18 m, the flight altitude is 30 m, the flight speed varies among 30, and 22, and 38 m/s, and the number of turns to each side varies among 8, 6, and 10 with the flight speed to achieve 100-second simulations for all cases.

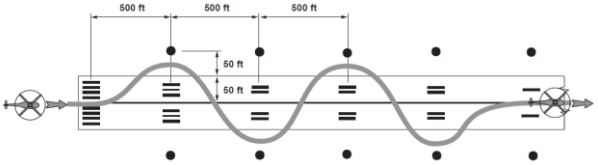

Fig. 7 Suggested course for slalom MTE[31]

Table 1 Flight path setup

Case no.	y_s (m)	h (m)	$V(m/s)$	n_{trn}
1-3, 6-7, 10-11, 13, 15	18	30	30	8
4, 8-9, 12, 14	18	30	22	6
5	18	30	38	10

4.2. Turbulent Wind Conditions

Table 2 presents the turbulent wind conditions. Cases 1-3 are simulated without turbulent wind to validate the accuracy of the pilot model for manoeuvring flight and the airspeed is 30 m/s to meet the level-1 performance requirements. The remainders are set with the mean wind speed of 8 m/s. Cases 4-7 are used to check the effect of mean wind on rotorcraft handling qualities by varying the wind directions among 0, 180, 90, and 270 degrees regardless of turbulence. However, the airspeed remains the same as 30 m/s by changing the ground speed, as shown in Table 2. Cases 8-11 aim to investigate the effect of atmospheric turbulence by varying the vertical turbulence intensity between 0.7 and 1.2 m/s with the wind direction of 0 deg for the first two cases and 180 deg for the latter two cases. The airspeed for Cases 8-9 is 30 m/s and for Cases 10-11 is 22 m/s. Cases 12-15 are targeted to investigate the effect of flight control system, and the turbulent wind conditions for Cases 12 and 14 are repeated from Case 9, while those for Cases 13 and 15 remain the same as Case 11.

4.3. Development of Flight Control System

A simple Flight Control System (FCS) is developed from the stability augmentation system of the UH-60A helicopter[37] for the simulation of Cases 3 and 12-15. The authority of the FCS is originally limited to 10% for all three angular rate feedback channels, and the transfer functions are

$$(34)\ \frac{\delta_{\text{lat}}^{\text{sas}}}{p}(s) = \frac{206.754(s+1.5704)}{s^3+33.1652s^2+534.1544s+520.9001}+\frac{0.278}{s}$$

$$(35)\ \frac{\delta_{\text{lon}}^{\text{sas}}}{q}(s) = \frac{307.462(s+1.1254)}{s^3+24.2029s^2+298.2384s+160.9515}\frac{7s}{7s+1}$$

$$(36)\ \frac{\delta_{\text{ped}}^{\text{sas}}}{r}(s) = \frac{434.5613}{s^2+34.3147s+390.1332}\frac{2s}{2s+1}$$

where $\delta_{\text{lat}}^{\text{sas}}/p$, $\delta_{\text{lon}}^{\text{sas}}/q$, and $\delta_{\text{ped}}^{\text{sas}}/r$ are the flight control system transfer functions for the roll, pitch, and yaw channels in %/deg.

Table 3 shows the FCS setup. The FCS for Cases 3 and 12-13 is set with full authority, while that for Cases 14-15 is set with the original 10% authority. The vestibular system is activated for the proposed pilot model in all cases except Case 1. The preview time for the pilot trajectory tracking laws varied among 1.7, 1.6, and 1.5 s according to the operating conditions of the pilot vestibular system and FCS to achieve the minimum tracking error for each case.

Table 2 Turbulent wind setup

Case no.	$U_{30}(m/s)$	$\psi_w(deg)$	$\sigma_{\text{w}}(m/s)$	V_{A}(m/s)
1-3	0	0	0	30
4	8	0	0	30
5	8	180	0	30
6	8	90	0	30
7	8	270	0	30
8	8	0	0.7	30
9,12,14	8	0	1.2	30
10	8	180	0.7	22
11,13,15	8	180	1.2	22

Table 3 Flight control system setup

Case no.	FCS	Vestibular	τ_{p}(s)
1	Off	Off	1.7
2, 4-11	Off	On	1.6
3, 12-13	On, 100%	On	1.5
14-15	On, 10%	On	1.5

5. MODEL ACCURACY ASSESSMENT

The accuracy of the proposed pilot model will be assessed by a linear version of the flight dynamics model and nonlinear simulation of the slalom MTE for Cases 1-3 based on the following methodology for HQs evaluation.

5.1. Methodology for Handling Qualities Evaluation

The tracking performance for each case is quantitatively estimated by defining the standard error $\sigma_{\Delta y}$ between the simulated and desired lateral distances at the turning points,

$$(37)\ \sigma_{\Delta y} = \sqrt{\frac{1}{n_{\text{s}}\cdot 2n_{\text{trn}}}\sum_{i=1}^{n_{\text{s}}}\sum_{j=1}^{2n_{\text{trn}}}\left(y_{i,j}-y_{\text{s}}\right)^2}$$

where n_s is the number of simulations for each case; $y_{i,j}$ is the distance from the centreline at the jth turn of the ith simulation.

The HQs levels are predicted by the Handling Qualities Sensitivity Function (HQSF)[16]. Hess postulates that a pilot's perception of a vehicle's HQs is dependent upon the power in the proprioceptive feedback signal U_{M} as shown in Fig. A1. In view that U_{M} is dependent upon the transfer function U_{M}/C, this function is normalized by the visual feedback gain K_Φ to remove the effects of control sensitivity and then the magnitude is referred as the HQSF,

$$(38)\ \text{HQSF} = \frac{1}{K_\Phi}\left|\frac{U_M}{C}(j\omega)\right|$$

where C represents the visual tracking signal of the compensatory pilot model.

The HQSF can be easily obtained for a linear flight dynamics model [8]. It can be expanded to the HQs evaluation for nonlinear simulation by three steps. First, 100 simulations are conducted for each case to remove randomness due to pilot's visual error and turbulence disturbance. Then, the Power Spectral Densities (PSD) of the visual tracking and proprioceptive feedback signals are calculated for each simulation. Finally, the averages of the PSDs are estimated to calculate the HQSF by Eq. (38).

5.2. Results

Figure 8 shows the HQ results by the linear flight dynamics model. In Case 1 the HQs for the four control channels are Level 2 (Lateral), Level 3 (Longitudinal), Level 1 (Vertical), and Level 3 (Yaw), resulting in a Level-3 HQs for the bare-frame vehicle due to the poorest result in the longitudinal and yaw axes. Compared to Case 1, with the vestibular cues in Case 2, better results are achieved in all four axes, and the HQs for the object rotorcraft is improved to Level 2. This is because the pilot needs less time to perceives vehicle rate responses from a combination of the vestibular and visual cues than just the visual cues, which helps to reduce the time delay and improve the crossover frequency for the man/machine system[37]. As a result, the increased system stability and control bandwidth improve the HQ levels[13]. Furthermore, a comparison between Cases 2 and 3 reveals that the flight control system significantly improves the HQs to Level 1 in all axes. Figures 9 compare the simulated flight paths and lateral distance standard errors among Cases 1-3. The desired flight path is smoothly programmed and well tracked by the proposed pilot model with the tau guidance strategy. A slight improvement in the tracking performance (by approximately 9%) is revealed when the vestibular system is enabled. This is to be expected due to the larger bandwidth[13].

Furthermore, the pilot model captures the effect of the flight control system on the significant improvement in the tracking performance (by approximately 33%).

Figure 10 shows a slice of the visual tracking and proprioceptive feedback signals by the proposed pilot model. In Case 1 when the vestibular system is broken, the proprioceptive signals are significantly oscillating at a medium frequency, indicating instability in the man/machine system. In comparison, the proprioceptive signals in Case 2 are much smoother without undesired oscillations, demonstrating that the proposed pilot model simulates the improved stability in the man/machine system by enabling the vestibular system. Case 3 demonstrates that the pilot model captures the effect of the flight control system on the improvement of stability to the man/machine system.

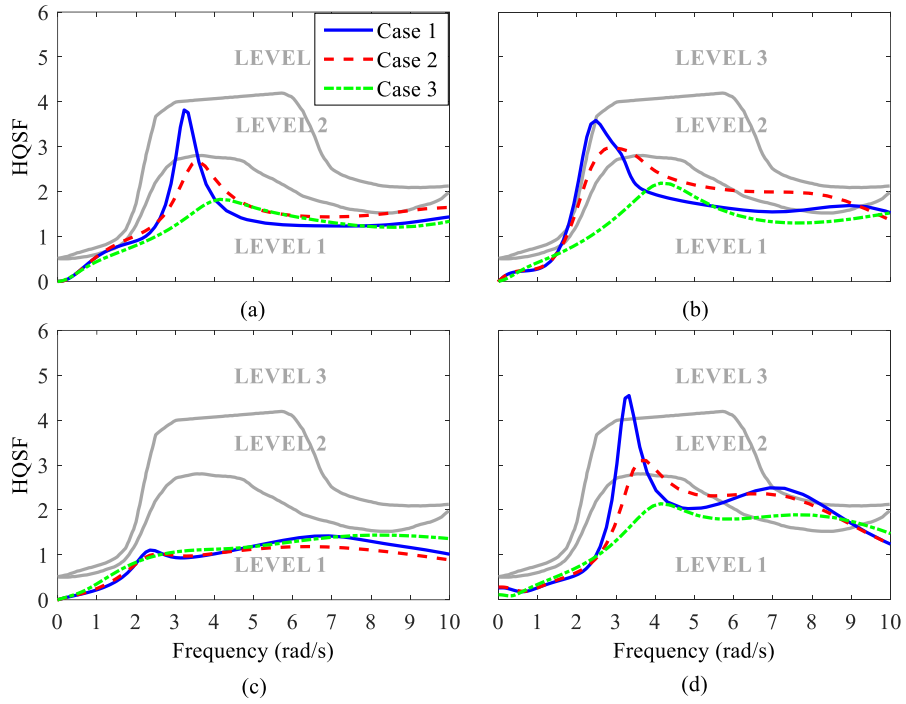

Fig. 8 Handling qualities results by a linear flight dynamics model. (a) lateral; (b) longitudinal; (c) vertical; (d) yaw

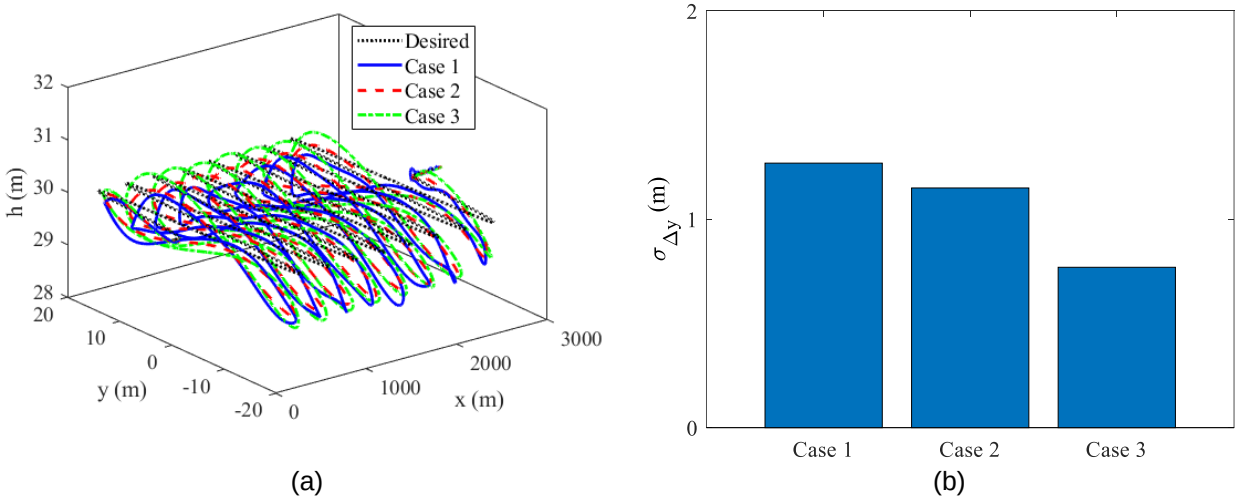

Fig. 9 Comparison of (a) simulated flight path and (b) lateral distance standard error

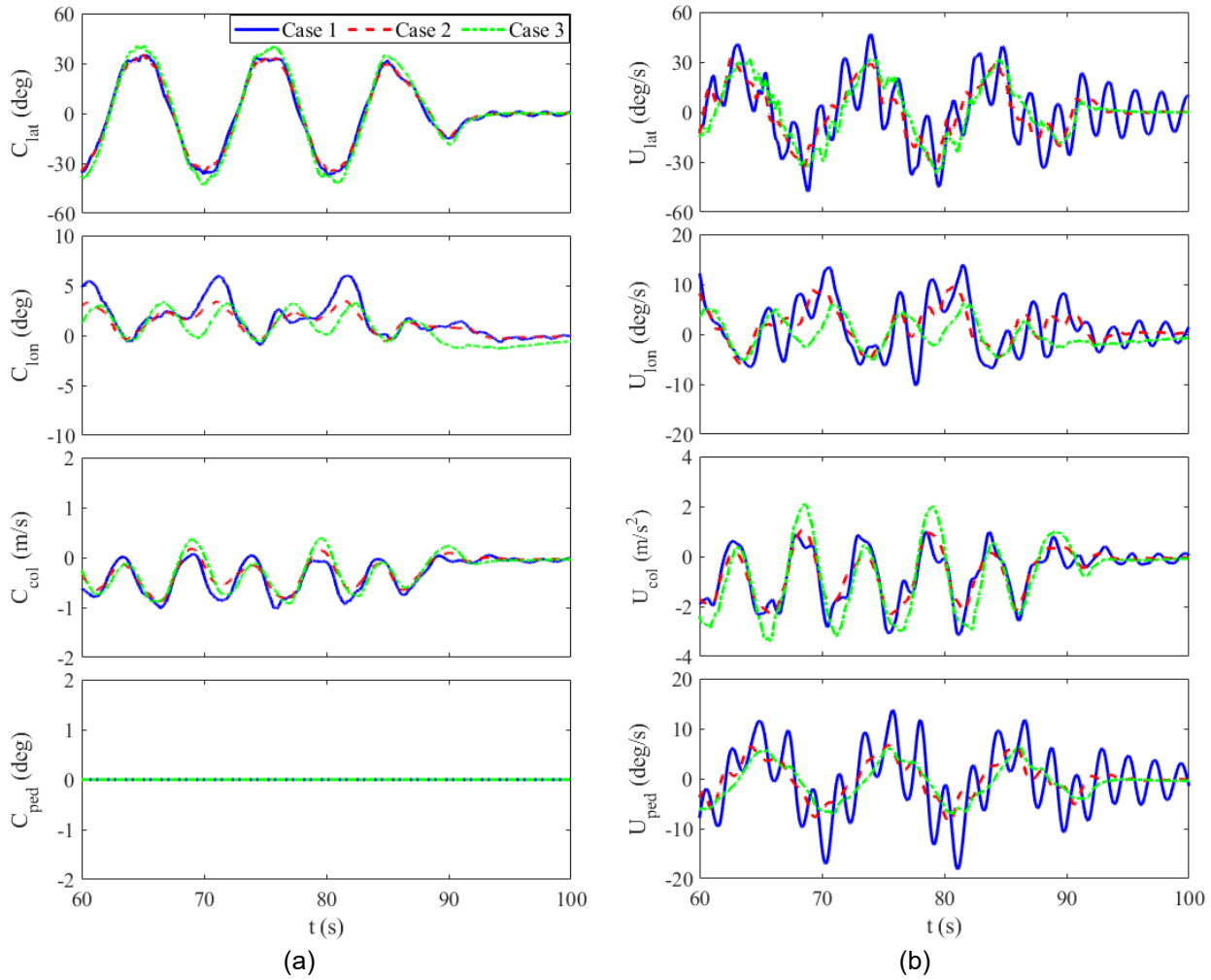

Fig. 10 Tracking and feedback signals for handling qualities evaluation

Figure 10 further reveals two features in the pilot control strategy for the slalom MTE. One is that the visual tracking and proprioceptive signals for the lateral control are much larger than those for the longitudinal, vertical, and yaw channels, as expected that this is a lateral control dominant trajectory tracking task and the pilot relies on the lateral motion cue to accomplish this task[33]. The other is that the visual tracking signals are much smaller than the proprioceptive signals in the longitudinal, vertical, and yaw axes. The result indicates that the proprioceptive systems are mainly used to compensate the inter-axis responses suffering from the lateral control rather than relying on the visual signals from the outer loops[39] since the desired ground speed, vertical position, and sideslip angle remain constant during the manoeuvre. Therefore, the lateral control is primarily responsible for the HQs while the other axes are secondly important to coordinate with the primary control.

Figure 11 compares the simulated lateral HQSFs among Cases 1-3. The lateral HQs are Level 2 when the vestibular feedback is broken and are improved to Level 1 when the vestibular and flight control systems are enabled. The results have a good agreement with the analytical results in Fig. 8(a) and the desired tracking performance in Fig. 9.

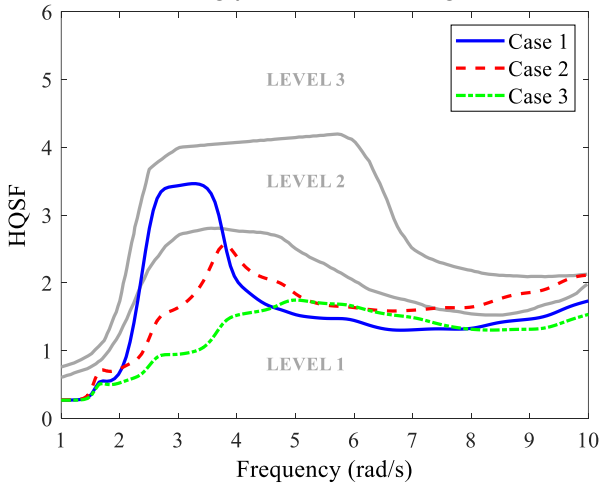

Fig. 11 Comparison of simulated lateral HQSF

The above results demonstrate that the effect of the manoeuvre and turbulent wind on HQs can be investigated by comparing the lateral HQSFs when

performing the Slalom MTE and the proposed pilot model can predict credible HQSFs for the HQs evaluation of specific MTE.

6. HANDLING QUALITIES ANALYSIS IN TURBULENT WIND

In this Section, the Slalom MTE was simulated for Cases 4-15 and the corresponding lateral HQSFs were calculated to show the effect of turbulent wind on the HQs. The results are given here.

6.1. Effect of Mean Wind

Figure 12 reveals the effect of mean wind on the simulated flight path and lateral distance standard error by Cases 4-7. Compared with Case 2 in a calm atmosphere in Fig. 9, the east wind results in the worst tracking performance, the south wind results in the second worse performance, the west wind has nearly no effect, and the north wind improves the manoeuvre. The north and south wind results match well with the ground speed varying from 22 m/s to 38 m/s in that the trajectory is tracked less aggressively by a smaller ground speed. The east wind is opposite to the direction of the tail rotor thrust and makes the helicopter tend to turn right resulting in a right shift on the flight path, as shown in Fig. 12(a). The west wind is along with the direction of tail rotor thrust and makes it easier for the yaw control.

Figure 13 demonstrates the effect of mean wind on the lateral HQSFs. The manoeuvers in mean wind require more high-frequency operations leading to worse HQSFs for all cases compared to Case 2 in a calm atmosphere. Furthermore, the predicted operation in south wind is much more aggressive resulting in a worse HQSF than that in north wind, and east wind makes it harder for yaw operation and results in a bit worse lateral HQSF than that in west wind.

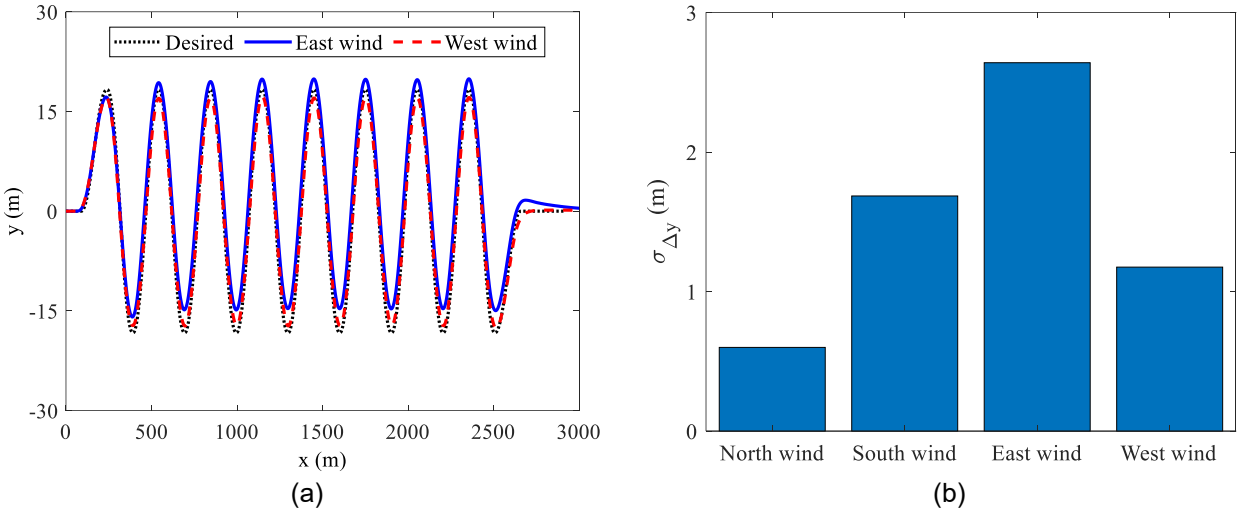

Fig. 12 Effect of mean wind on (a) simulated flight path and (b) lateral distance standard error

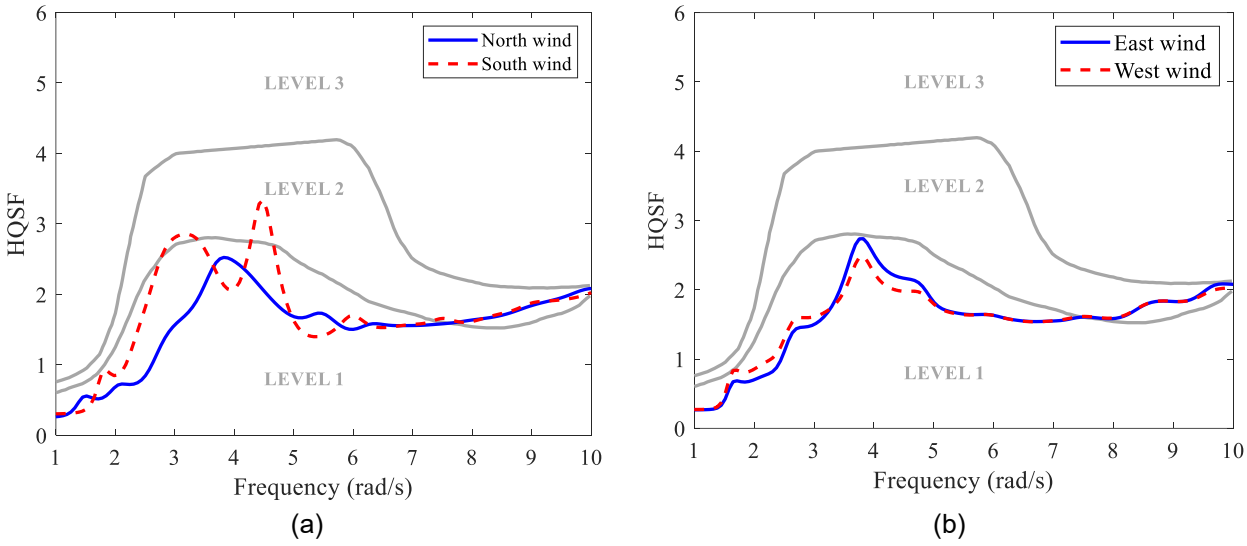

Fig. 13 Effect of mean wind on lateral HQSF

6.2. Effect of Atmospheric Turbulence

Figure 14 shows the effect of atmospheric turbulence on the flight path by Cases 8-11. It can be observed that the turbulence disturbances increase the lateral distance errors that were estimated for each case, as presented in Fig. 12. The lateral distance standard errors for north and south wind conditions increase as well with the increased turbulence intensities.

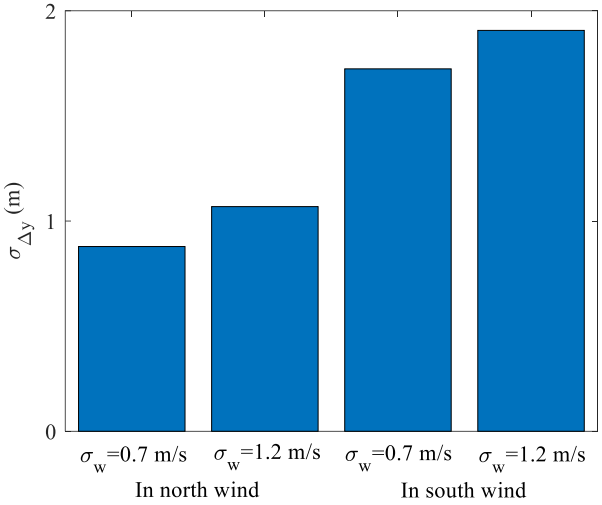

Fig. 14 Effect of atmospheric turbulence on lateral distance standard error

The corresponding lateral HQSFs are compared in Fig. 15. It can be found that atmospheric turbulence significantly increases the lateral HQSFs in the medium-frequency with the increased turbulence intensity compared with the same wind conditions shown in Fig. 13(a) but without turbulence. Fig. 15(b) shows the lateral HQs deteriorate with the increased turbulence intensity. However, the HQs in south wind with the ground speed of 30 m/s are better than those in north wind with the ground speed of 22 m/s, indicating that rotorcraft HQs are more sensitive to the effect of turbulent wind at low speeds than at high speeds.

6.3. Effect of Flight Control System

Figure 16 shows the effect of the flight control system on the lateral distance standard error by Cases 12-15. Compared with the same turbulent wind conditions in Fig. 14, the inclusion of the flight control system improves the tracking performance for the north wind cases by 20% while the lateral standard error is reduced from 1.1 m/s to 0.8 m/s. The result at the south wind condition with a full-authority flight control system is even better with the lateral standard error reduced by more than 30% from 1.9 m/s to 1.3 m/s. However, the south wind case with inadequate authority shows poor performance as the lateral distance standard error is increased by 38% from 1.3 m/s to 1.8 m/s. This can be explained by the required flight control outputs in Fig. 17, which are significantly increased to be larger than the authority in about half of the operations when the ground speed increases from 22 to 30 m/s. The 10%-authority is inadequate to complete the manoeuvre as aggressively as with a ground speed up to 30 m/s, making the effect of the flight control system heavily discount.

Figure 18 presents the corresponding lateral HQSFs to reveal the effect of the flight control system on the HQs. The flight control system significantly improves the HQs from Level 3 to Level 1 for the north wind cases and from Level 2 to Level 1 for the south wind cases. Furthermore, compared between the full-authority cases in south wind condition, it is evident that the reduced authority deteriorates the HQs although they are still in Level 1 region.

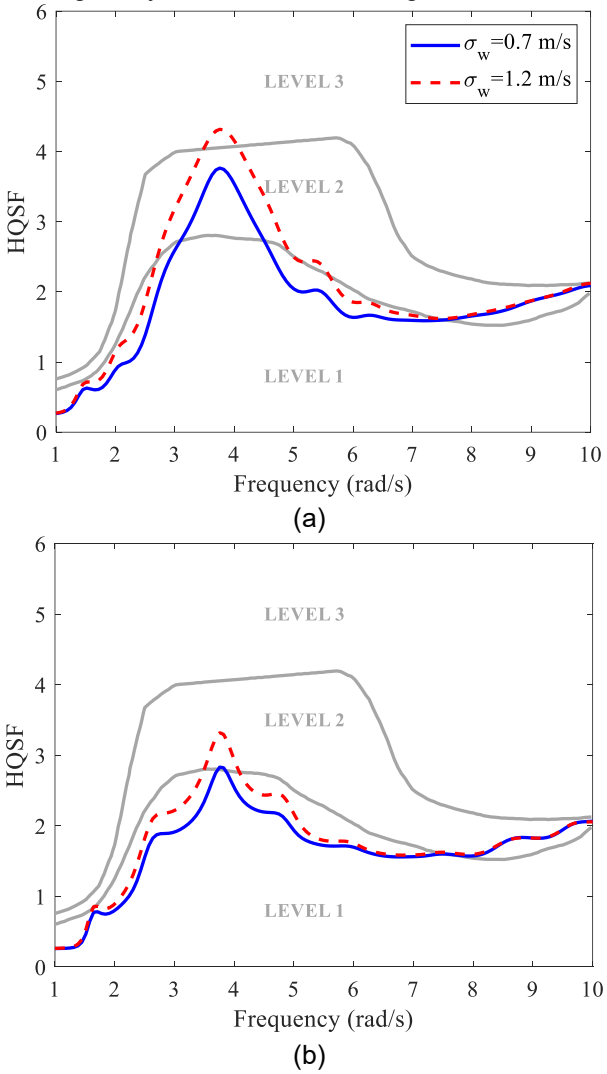

Fig. 15 Effect of turbulence on lateral HQSF in (a) north and (b) south wind conditions

7. DISCUSSION

Trajectory planning and tracking conforming to the guidance strategy of a human pilot has become an obstacle on the state-of-the-art pilot models for HQs investigation. Recent progress in bio-inspired optic theory[25-27] and preview control behaviour[14] from

piloted experiments provide a good opportunity to solve these problems. It was shown that the proposed pilot model could predict credible HQs capturing the effect of the vestibular system and flight control system. The nonlinear simulation results suggested that the proposed pilot model could plan and track a desired trajectory conforming to pilot's tau guidance strategy. Analysis of the visual tracking and proprioceptive signals revealed that the pilot control inputs from the tracking-control channel were primarily responsible for the HQs of a manoeuvring flight while the other channels employed a compensatory control strategy to reject the inter-axis coupling responses and atmospheric disturbances and were secondly important for the HQs. This work gives the first try to improve the structural pilot model with a tau guidance law and a preview control strategy for manoeuvring flight simulations, providing a convenient desktop tool for rotorcraft HQs investigation.

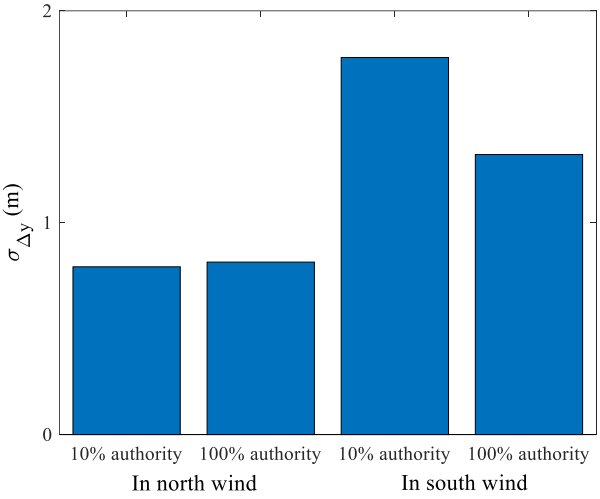

Fig. 16 Effect of flight control system on lateral distance standard error

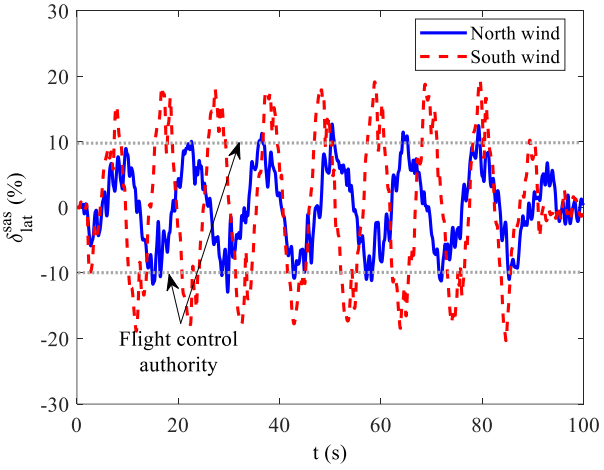

Fig. 17 Effect of turbulent wind on required flight control outputs

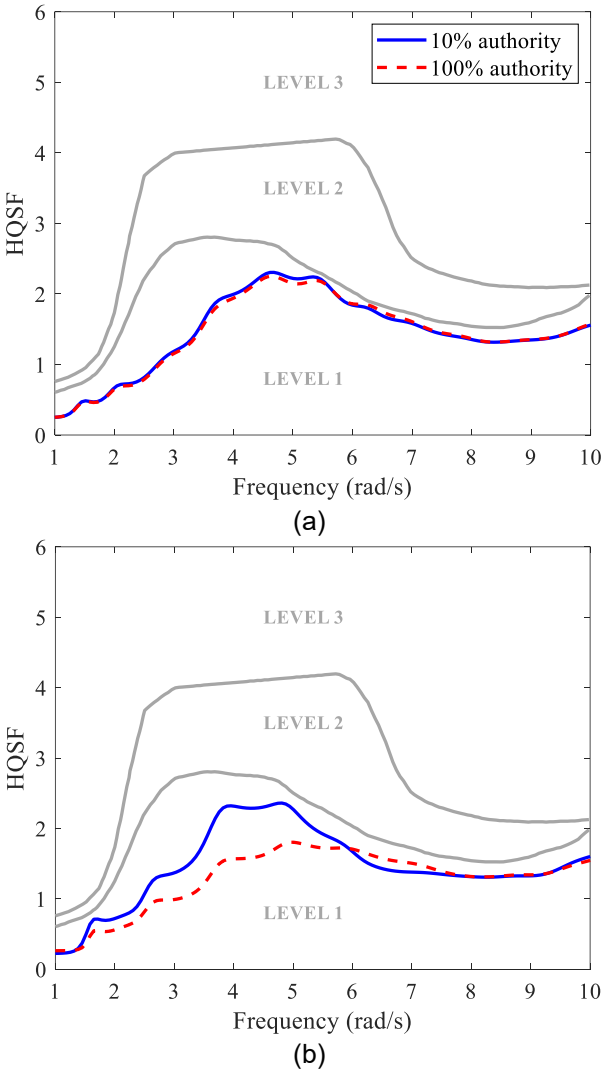

Fig. 18 Effect of fight control system on lateral HQSF in (a) north and (b) south wind conditions

The effect of turbulent wind on rotorcraft HQs was investigated via simulation of the slalom MTE. The comparison between cases in mean wind conditions showed that headwind could improve the tracking performance and HQs by reducing the ground speed, and tailwind, in contrast, significantly deteriorated the task. Side wind opposite to the direction of tail rotor thrust would lead to a lateral shift from the desired path. The comparison between cases in turbulent wind conditions showed that atmospheric turbulence led to the deteriorated tracking performance and HQs with the increased turbulence intensities. The simulation results for the augmented UH-60A helicopter revealed that the stability augmentation system could significantly improve the tracking performance and HQs in turbulent wind. However, the saturation due to the limited authority would deteriorate the effect of the flight control system as the ground speed was up to 30 m/s. Danger could be warned if the ground speed was further increased to complete the task more

aggressively. The effect of turbulent wind on rotorcraft HQs is a long-term care topic. The ultimate aim is to establish turbulence stipulations for rotorcraft applications, which are still absent in the forthcoming version of rotorcraft HQs performance specification ADS-33F-PRF[31].

One deficiency of this research is that the effect of turbulent wind on the HQs is investigated by only the lateral HQSF while the other channels, though are secondly important, may also have a bit impact on the HQs[39]. Another is that the results for cases with flight control saturation may be distorted due to the pilot model. Future work will continue to repair the deficiencies and expand the research into more MTEs required in ADS-33F-PRF.

8. CONCLUSIONS

This paper developed a pilot model for rotorcraft manoeuvring simulation in turbulent wind and the corresponding HQs investigation. The proposed pilot model consists of inner-loop compensatory control laws for attitude stabilization, outer-loop preview control laws for trajectory tracking, and tau guidance laws for trajectory planning. The pilot model was integrated into an incorporated turbulent wind and flight dynamics model and the slalom MTE was simulated to investigate the effect of turbulent wind on rotorcraft HQs. The following conclusions can be drawn.

1) The proposed pilot model can plan and track a desired trajectory conforming to the tau guidance strategy and the corresponding HQs are credibly predicted capturing the effect of the vestibular system and flight control system.
2) The pilot control inputs from the tracking-control channel are primarily responsible for the HQs of a manoeuvring flight while the other channels employ a compensatory control strategy to reject the inter-axis coupling responses and atmospheric disturbances and are secondly important for the HQs.
3) Mean wind has an important effect on the HQs and tracking performance. Head wind is favourable in that it reduces the required ground speed and thus the manoeuvre is performed less aggressively. By contrast, tail wind is adverse due to the increased ground speed. Side wind opposite to the direction of tail rotor thrust makes the yaw operation more difficult toward main rotor rotational direction.
4) Atmospheric turbulence deteriorates the performance and HQs with the increased turbulence intensities. Flight control systems as simple as a stability augmentation system can significantly improve the tracking performance and HQs in turbulent wind but the saturation due to the limited authority in aggressive operation conditions reduces the effect of the flight control system.

ACKNOWLEDGEMENTS

This work was supported by the National Natural Science Foundation of China (Grant Number: 11902052), the Chongqing Science and Technology Commission (Bureau) (Grant Number: cstc2019jscx-msxmX0043), the National Key Laboratory of Rotorcraft Aeromechanics (Grant Number: JZX7Y201911SY004001), and the Open Project of Rotor Aerodynamics Key Laboratory (Grant Number: RAL20190201).

REFERENCES

[1] Ji H., Chen R., Lu L, White M. D., “Pilot Workload Investigation for Rotorcraft Operation in Low-Altitude Atmospheric Turbulence”, Aerospace Science and Technology, Vol. 111, 2021, pp. 106567.

[2] Lusardi, J. A., Tischler, M. B., Blanken, C. L., and et al., “Empirically Derived Helicopter Response Model and Control System Requirements for Flight in Turbulence”, Journal of the American Helicopter Society, Vol. 49, No. 3, 2004, pp. 340-349.

[3] Ji H., Chen R., Li P., “Distributed Atmospheric Turbulence Model for Helicopter Flight Simulation and Handling-Quality Analysis”, Journal of Aircraft, Vol. 54, No. 1, 2017, pp. 190-198.

[4] Ji H., Chen R., Li P., “Distributed Turbulence Model with Accurate Spatial Correlations for Simulation of Helicopter Flight in Atmospheric Turbulence”, Journal of the American Helicopter Society, Vol. 64, 2019, pp. 042011.

[5] Ji H., Chen R., Li P., “Real-Time Simulation Model for Helicopter Flight Task Analysis in Turbulent Atmospheric Environment”, Aerospace Science and Technology, Vol. 92, 2019, pp. 289-299.

[6] Cameron N., White M. D., Padfield G. D., Lu L., Agarwal D., Gubbels A. W., “Rotorcraft Modeling Renovation for Improved Fidelity”, Vertical Flight Society 75th Annual Forum, Philadelphia, USA, May 2019, pp. 13-16.

[7] McRuer D. T., Clement W. F., Thompson, Magdaleno, R. E., “Minimum Flying Qualities Volume II: Pilot Modelling for Flying Qualities Application”, Flight Dynamics Lab., Air Force Systems Command, Wright–Patterson AFB, WRDC-TR-9-3100, Jan. 1990.

[8] Davidson J., Schmidt D. K., “Modified Optimal Control Pilot Model for Computer-Aided Design and Analysis,” NASA TM 4384, 1992.

[9] Doman D., “Projection Methods for Order Reduction of Optimal Human Operator Models,” Ph.D. Dissertation, Virginia Polytechnic Institute and State University, 1998.

[10] Lone M., “Pilot Modelling for Airframe Loads Analysis,” Ph.D. Dissertation, University of Cranfield, May 2013.

[11] Hosman R., “Pilot’s Perception & Control of Aircraft Motions”, Ph.D. Dissertation, Delft University of Technology, November 1996.
[12] Hess R. A., Zeyada Y., Heffley R. K., “Modeling and Simulation for Helicopter Task Analysis”, Journal of the American Helicopter Society, Vol. 47, No. 4, 2002, pp. 243-252.
[13] Lu, L., Jump, M., “Multiloop Pilot Model for Boundary-Triggered Pilot-Induced Oscillation Investigations”, Journal of Guidance, Control, and Dynamics, Vol. 37, No. 6, 2014, pp. 1863-1879.
[14] van der El K., Pool D. M., van Paassen M. R. M., et al., “Effects of Preview on Human Control Behavior in Tracking Tasks with Various Controlled Elements”, IEEE transactions on cybernetics, Vol. 48, No. 4, 2017, pp. 1242-1252.
[15] Hess R. A., Chan K., “Preview Control Pilot Model for Near-Earth Manoeuvreing Helicopter Flight”, Journal of Guidance, Control, and Dynamics, Vol. 11, No. 2, 1988, pp. 146-152.
[16] Hess R. A., “Unified Theory for Aircraft HQs and Adverse Aircraft-Pilot Coupling”, Journal of Guidance, Control, and Dynamics, Vol. 20, No. 6, 1997, pp. 1141-1148.
[17] Hess, R. A., and Siwakosit, W., “Assessment of Flight Simulator Fidelity in Multiaxis Tasks Including Visual Cue Quality,” Journal of Aircraft, Vol. 38, No. 4, 2001, pp. 607–614.
[18] Hess R. A., Marchesi F., “Analytical Assessment of Flight Simulator Fidelity Using Pilot Models”, Journal of Guidance, Control, and Dynamics, Vol. 32, No. 3, 2009, pp. 760-770.
[19] Ji H., Chen R., Li P., “Rotor-State Feedback Control to Alleviate Pilot Workload for Helicopter Shipboard Operations”, Journal of Guidance, Control, and Dynamics, Vol. 40, No. 12, 2017, pp. 3088-3099.
[20] Lee D., Sezer-Uzol N., Horn J. F., et al., “Simulation of Helicopter Shipboard Launch and Recovery with Time-Accurate Airwakes”, Journal of Aircraft, Vol. 42, No. 2, 2005, pp. 448-461.
[21] Thomson D. G., Bradley R., “Mathematical Definition of Helicopter Manoeuvres”, Journal of the American Helicopter Society, Vol. 42, No. 4, 1997, pp. 307-309.
[22] Thomson D., Bradley R., “Inverse Simulation as a Tool for Flight Dynamics Research—Principles and Applications”, Progress in Aerospace Sciences, Vol. 42, No. 3, 2006, pp. 174-210.
[23] Lee, D. N., “Guiding Movement by Coupling Taus,” Ecological Psychology, Vol. 10, No. 3, 1998, pp. 221–250.
[24] Lee, D. N., “Tau in Action in Development,” Action as an Organizer of Learning and Development, Vol. 33, Minnesota Symposium on Child Psychology, edited by J. J. Rieser, J. J. Lockman, and C. A. Nelson, Psychology Press, Hove, England, U.K., 2005, pp. 3–50.
[25] Padfield G. D., Clark G., Taghizad A., “How Long Do Pilots Look Forward? Prospective Visual Guidance in Terrain‐Hugging Flight”, Journal of the American Helicopter Society, Vol. 52, No. 2, 2007, pp: 134-145.
[26] Padfield G. D., “The Tau of Flight Control”, The Aeronautical Journal, Vol. 115, No. 117, 2011, pp. 521-556.
[27] Lu L., Jump M., Padfield G. D., “Development of a Generic Time-to-Contact Pilot Guidance Model”, Journal of Guidance, Control, and Dynamics, Vol. 41, No. 4, 2018, pp. 904-915.
[28] Counihan J. O., “Adiabatic Atmospheric Boundary Layers: A Review and Analysis of Data from the Period 1880–1972”, Atmospheric Environment, Vol. 9, No. 10, 1967, pp. 871-905.
[29] Gualtieri G., “Surface Turbulence Intensity as a Predictor of Extrapolated Wind Resource to the Turbine Hub Height”, Renewable Energy, Vol. 78, 2015, pp. 68-81.
[30] Etkin B., Dynamics of Atmospheric Flight, John Wiley and Sons, Inc., New York, USA, 1972, Chapter 13.
[31] Blanken, C. L., Tischler, M. B., Lusardi, J.A., et al, “Proposed Revisions to Aeronautical Design Standard – 33E (ADS-33E-PRF) Toward ADS-33F-PRF,” U.S. Army Combat Capabilities Development Command, Special Report FCDD-AMV-19-01, September 2019.
[32] Anon., “Helicopter Flying Handbook (FAA-H-8083-21B)”, United States Department of Transportation, Federal Aviation Administration, Oklahoma, 2019.
[33] Agarwal D., Lu L., Padfield G. D., White M. D., Cameron, N., “Rotorcraft Lateral-Directional Oscillations: The Anatomy of a Nuisance Mode,” Journal of the American Helicopter Society, Vol. 66, 2021, pp. 042000.
[34] Padfield G. D., Helicopter Flight Dynamics: The Theory and Application of Flying Qualities and Simulation Modelling, John Wiley & Sons, 2008, Chapter 3.
[35] Jump M., Padfield G D., “Investigation of the Flare Manoeuvre Using Optical Tau”, Journal of Guidance, Control, and Dynamics, Vol. 29, No. 5, 2006, pp. 1189-1200.
[36] Padfield G., White M., “Measuring simulation fidelity through an adaptive pilot model”, Aerospace Science and Technology, Vol. 9, No. 5, 2005, pp. 400-408.
[37] Howlett, J. J., “UH-60A Black Hawk Engineering Simulation Program”, NASA CR-166309, Washington, D.C., 1981.
[38] McRuer D. T., Krendel E. S., “Mathematical Models of Human Pilot Behavior”, AGARDograph AG-188, AGARD, November 1973.

[39] Memon W. A., White M. D., Padfield G. D., Cameron N., Lu L., “Helicopter Handling Qualities: A study in Pilot Control Compensation,” Aeronautical Journal, 2021, in print.

Presented at 47th European Rotorcraft Forum, United Kingdom, 7-9th September, 2021